RSC Advances

PAPER

View Article Online
View Journal | View Issue

Cite this: *RSC Adv.*, 2020, **10**, 40948

A study on the selective catalytic reduction of NO_x by ammonia on sulphated iron-based catalysts

Caixia Liu, *[a] Huijun Wang,[a] Yalian Bi[a] and Ziyin Zhang[b]

A series of sulphated iron-based catalysts was prepared *via* an impregnation method by changing the loading content of Fe^{3+} and SO_4^{2-} on ZrO_2, and their performance in the selective catalytic reduction (SCR) of NO_x by ammonia was investigated. The NO_x conversion exhibited large differences among the sulphated iron-based catalysts. To explore the synergistic mechanism of iron and sulphates, XRD, BET, H_2-TPR, XPS, TPD and *in situ* DRIFTS were used to characterize the catalysts, and it was found that among all the catalysts, the NO_x conversion by Fe_2SZr was greater than 90% at 350–450 °C. The results indicated that the interaction between Fe^{3+} and SO_4^{2-} can have an effect on the redox ability, acid sites, and adsorption of NO_x and NH_3. With an increase in the content of Fe^{3+}, the redox activity of the catalyst and the adsorption of ammonia improved at medium and low temperatures. However, at higher temperatures, an increase in Fe^{3+} led to a decrease in the conversion of NO_x due to the enhanced oxidation of NH_3. At medium and low temperatures, an increase in the content of SO_4^{2-} decreased the concentration of Fe^{3+} on the surface of the catalyst and inhibited the adsorption of NO_x and NH_3. The addition of SO_4^{2-} reduced the redox activity of the catalyst and inhibited the oxidation reaction of NH_3, which follows the Eley–Rideal mechanism at high temperatures, further enhancing the SCR activity of the Fe_xS_yZr catalyst.

Received 3rd August 2020
Accepted 8th October 2020

DOI: 10.1039/d0ra06697d

rsc.li/rsc-advances

1. Introduction

The temperature of the waste gas of a bituminous coal-fired power plant is generally 300–450 °C.[1,2] In particular, the temperature after burning lignite reaches up to 420 °C. Also, under conditions with a high sulphur content, the commercially available catalysts (vanadium-based catalysts) show low denitrification activity and poor N_2 selectivity, which make them easily poisoned and secondary pollution being released into the environment.[3–6] Therefore, it is urgent to develop environment-friendly catalysts with sulphur resistance, high activity, and high N_2 selectivity at high temperature.[7–9]

Iron-based catalysts exhibit a good NO_x conversion rate and N_2 selectivity, and thus, have been favored by many researchers.[10–17] However, the selective catalytic reduction (SCR) activity of α-Fe_2O_3 catalysts at temperatures above 300 °C significantly decreases, and thus they cannot be applied in the denitrification of waste gas after burning coal. In recent years, some researchers attempted to improve the performance of catalysts by sulphating them. Gu *et al.*[18] carried out the sulphation of CeO_2 *via* a gas phase method, achieving a reaction activity of up to 99% in the temperature range of 300–500 °C. Ma *et al.*[19] prepared $Fe_2(SO_4)_3/TiO_2$ *via* impregnation, exhibiting a conversion rate of 97% and N_2O selectivity lower than 5% at 350–450 °C. Therefore, the sulphation of catalysts is a very effective way to improve their reactivity and N_2 selectivity at high temperature. According the literature,[20–25] the high catalytic efficiency and good sulfur resistance of catalysts upon acidification treatment can be mainly ascribed to the following reasons: (1) the reaction with the active material improves the transformation between the active material ion, increasing the reaction rate. (2) The number of Brönsted acid sites on the surface of the catalyst increases, increasing the strength of the acid sites, which is the main reason for the increase in catalytic activity. (3) Reaction with other substances on the catalyst to form sulfates, which enclose the active substances and reduce the sulphation of the active substances or act as active substances. Importantly, the NO_x conversion efficiency and N_2 selectivity of the sulphated catalysts improved.

To date, the synergistic mechanism between the active components and sulphates has not been reported. Therefore, we used Fe as an active component, which was sulphated and loaded onto a ZrO_2 carrier, to prepare a catalyst with a high NO_x conversion rate and high N_2 selectivity at high temperature. In this study, we loaded Fe^{3+} and SO_4^{2-} in different amounts on the ZrO_2 carrier *via* the impregnation method. The impact of Fe^{3+} and SO_4^{2-} loading on the performance of the NH_3-SCR catalyst was investigated using different characterization methods, and the synergistic mechanism of Fe^{3+} and SO_4^{2-} in the SCR reaction was discussed.

[a]*School of Environmental Science and Engineering, Tianjin University, Tianjin 300072, China. E-mail: liucx@tju.edu.cn; Fax: +86-22-8740-2075; Tel: +86-13426103078*
[b]*Langfang City Beichen Entrepreneurship Resin Materials Incorporated Company, Langfang 065000, China. E-mail: laowuzhangziyin@163.com; Tel: +86-15010892987*

2. Experimental

2.1 Catalyst preparation

All catalysts were prepared *via* the incipient wetness method. ZrO_2 power was weighed and dissolved in deionized water. Subsequently, $Fe(NO_3)_3 \cdot 9H_2O$ and $(NH_4)_2SO_4$ were added to the solution dropwise, and then heated to 70 °C and stirred to form a paste. The resulting mixture was dried at 120 °C overnight and calcined in air at 500 °C for 4 h. Finally, a series of iron-based catalysts was obtained, denoted as Fe_xS_yZr ($y = 5$, $x = 0$, 2, 3.5, 7 is denoted as Fe_xSZr and $x = 3.5$, $y = 0$, 5, 10, 15 is denoted as FeS_yZr; where x represents the weight percentage of Fe^{3+} and y represents the weight percentage of SO_4^{2-}).

2.2 Catalyst characterization

The gas concentration was detected using a Gasmet Dx-4000 FT-IR gas analyser, which can monitor NH_3, NO_2, NO, N_2O and water vapour. The reactant gas was 500 ppm NH_3, 500 ppm NO, 3% O_2 and N_2 balanced.

X-ray diffraction (XRD) measurements were performed on a D/MAX-RB system with Cu Ka radiation. The diffraction curves were measured in the 2θ range 10° to 90° with a step size of 0.018 at a rate of 1 s per step.

BET measurements were performed using a Quantachrome Autosorb AS-1 System using N_2 adsorption at 77 K.

X-ray photoelectron spectroscopy (XPS) was performed using an ESCALab220i-XL electron spectrometer with 300 W Mg Ka radiation under 3×10^{-9} mbar. The binding energies were calibrated using adventitious carbon with C 1s at 284.8 eV.

Temperature-programmed reduction (TPR) curves were measured using a Micromeritics ChemiSorb 2720. Firstly, the samples were preheated to 300 °C and maintained at a constant temperature for 1 h under N_2 purging and then cooled to 30 °C. The catalysts were reduced in a flow of N_2-based gas containing 10% H_2/Ar (50 cm^3 min^{-1}), and the temperature was programmed from 30 °C to 1000 °C at a heating rate of 10 °C min^{-1}.

Temperature programmed desorption (NH_3-TPD) experiments were conducted in an N_2-based mixture gas containing 500 ppm NH_3 (300 mL min^{-1}). The sample was preheated at 500 °C constantly for 1 h, then cooled to 30 °C, and NH_3 was introduced continuously for 1 h. Thirdly, the catalyst was blown with N_2 until to no NH_3 was detected. Finally, the catalyst was heated from 30 °C to 500 °C at a heating rate of 10 °C min^{-1}.

In situ DRIFTS spectra were characterized using a Nicolet NEXUS 870 FT-IR spectrometer. The sample was pre-treated at 300 °C for 1 h under a flow of N_2 (100 cm^3 min^{-1}).

3. Results and discussion

3.1 The effects on SCR activity with different loadings of Fe^{3+} and SO_4^{2-}

Fig. 1(a) shows the SCR activities of the SZr, Fe_2SZr, $Fe_{3.5}SZr$ and Fe_7SZr catalysts. According to this figure, the NO_x conversions of S_5Zr catalyst were very low in the temperature range of 150–500 °C and it reached the highest of 12% at 500 °C. Upon the addition of 2% Fe^{3+}, the NO_x conversions improved significantly, climbing rapidly from 10% at 250 °C to 90% at 350 °C, and reached the highest of 98% at 400 °C. Subsequently, with a further increase in the temperature to 500 °C, the NO_x conversion decreased to 57%. With a continuous increase in the loading of Fe^{3+}, the NO_x conversions were slightly higher than that of the Fe_2SZr catalyst in the temperature range of 250–350 °C, but they dropped significantly in the temperature range of 400–500 °C, which was negative at 500 °C.

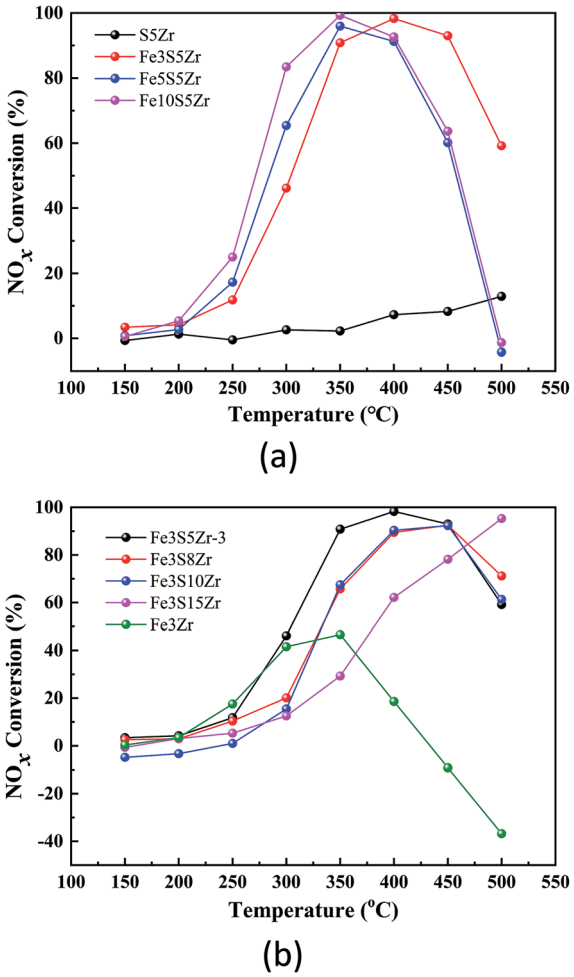

Fig. 1 (a) NO_x conversion of catalysts containing 5% SO_4^{2-} and x% Fe^{3+} ($x = 0$, 2, 3.5, 7). (b) NO_x conversion of catalysts containing 3.5% Fe^{3+} and y% SO_4^{2-} ($y = 0$, 5, 10, 15).

Fig. 1(b) shows the NO_x conversions by the FeZr, FeS_5Zr, $FeS_{10}Zr$ and $FeS_{15}Zr$ catalysts in the temperature range of 150–500 °C. According to this figure, the NO_x conversions of the FeZr, FeS_5Zr and $FeS_{10}Zr$ catalysts increased initially and then declined in the temperature range of 150–500 °C. The NO_x conversions of the FeZr catalyst were very close to that of the FeS_5Zr catalyst in the temperature range of 150–300 °C, which reached the peak of 46% at 350 °C, and then dropped sharply to a negative value from 400 °C to 500 °C. Upon the loading of SO_4^{2-}, the NO_x conversions improved in the high temperature range. When 10% SO_4^{2-} was added to the catalyst, the NO_x conversions were reduced in the temperature range of 250–450 °C compared with that of the FeS_5Zr catalyst. With the

further addition of SO_4^{2-} to 15%, the NO_x conversion exhibited an increasing trend from 150 °C to 500 °C, which was much lower than that of the FeS_5Zr catalyst in the range of 150–450 °C but it reached close to 100% at 500 °C.

3.2 Impact of Fe^{3+} and SO_4^{2-} loading on ammonia oxidation

Fig. 2(a) shows the curve of ammonia oxidation using a series of acidified catalysts in the temperature range of 150–500 °C. Accordingly, the SZr catalyst without Fe^{3+} loading started to oxidize NH_3 beginning at 400 °C and reached an NH_3 oxidation rate of 40% at 500 °C. However, it was reported that the self-oxidation reaction of NH_3 occurs when the temperature is higher than 400 °C, and thus, we speculated that a self-oxidation reaction mainly occurred on the SZr catalyst. With an increase in the loading amount of Fe^{3+}, the conversion of NH_3 oxidation shifted to a lower temperature, that is, the greater the loading amount of Fe^{3+}, the more the starting temperature of NH_3 oxidation was shifted to a lower temperature and the higher the corresponding oxidation rate of NH_3 in the temperature range of 300–450 °C. However, the NH_3 oxidation rates of the $Fe_{3.5}SZr$ and Fe_7SZr catalysts were close, indicating that although the higher the loading amount of Fe^{3+}, the higher the NH_3 oxidation rate, the NH_3 oxidation rate approached a constant at a certain temperature with a continuous increase in Fe^{3+}. In general, an increase in the amount of Fe^{3+} will promote the oxidation of NH_3 at high temperature. Combining the activities of the catalysts with varying amounts of Fe^{3+}, the NH_3 self-oxidation reaction mainly occurred on the Fe_2SZr, $Fe_{3.5}SZr$ and Fe_7SZr catalysts at 450–500 °C, which affected the efficiency of the catalytic reduction of the nitrogen oxides. Fig. 2(b) shows the changes in the curves of the NH_3 oxidation rate with the catalysts prepared by changing the content of sulphates. Accordingly, for the FeZr catalyst in the absence of sulphates, the oxidation reaction of NH_3 started from 250 °C, and the NH_3 oxidation rate reached 80% at 350 °C, while it reached 100% at 400 °C. Thus, based on the curve of the NH_3 oxidation rate for the FeZr catalyst, it can be concluded that in the temperature range of 350–500 °C, the NH_3 oxidation reaction mainly occurred on the FeZr catalyst, thus affecting the SCR reaction. With an increase in the sulphate content, the most efficient ammonia oxidation shifted to a higher temperature, that is, the addition of sulphates inhibited the oxidation reaction of NH_3 on the catalyst.

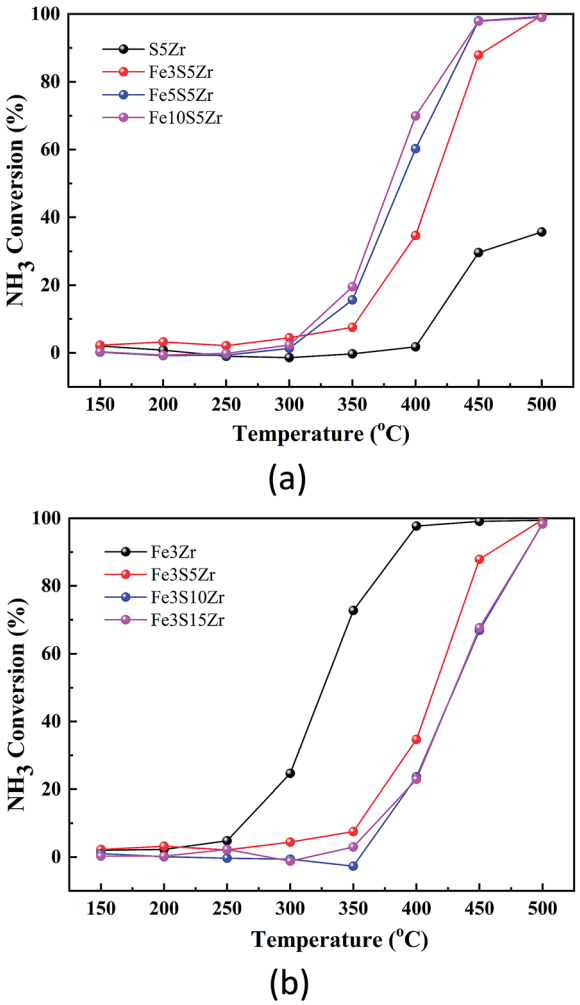

Fig. 2 (a) NH_3 oxidation efficiency of catalysts containing 5% SO_4^{2-} and x% Fe^{3+} (x = 0, 2, 3.5, 7). (b) The NH_3 oxidation efficiency of catalysts containing 3.5% Fe^{3+} and y% SO_4^{2-} (y = 0, 5, 10, 15).

3.3 H_2-temperature programmed reduction (TPR) analysis

The redox ability of catalysts is of great importance for the SCR reaction, which can be well characterized by H_2-temperature programmed reduction (TPR). Actually, the lower the temperature, the better the redox ability of the catalyst at low or medium temperatures.[26] The amount of hydrogen consumption is also an important indicator of the catalytic activity. The greater the hydrogen consumption, the stronger the redox capacity of the catalyst.[26–28] As shown in Fig. 3(a), there is only one H_2 reduction peak for the SZr catalyst at 583 °C, which is mainly attributed to the reduction peak of the sulphate species. According to the H_2-TPR curves of the series of Fe_2SZr catalysts, the reduction temperatures of the catalysts after the addition of Fe^{3+} were lower than that of SZr. The $Fe_{3.5}SZr$ and Fe_2SZr catalysts each showed only one redox peak, and these peaks were close to each other at 471 °C and 443 °C. These two reduction peaks are considered to be the completely overlapping reduction peaks of the iron oxide and the sulphates. The H_2-TPR redox curve of the Fe_7SZr catalyst has two reduction peaks at 425 °C and 473 °C. The former reduction peak can be attributed to the reduction peak of the iron oxide, while the peak at 473 °C is considered to be the overlapping reduction peaks of the iron oxide and the sulphates. As shown in Fig. 3(b), the H_2-TPR curve of the FeZr catalyst mainly has three reduction peaks at 330 °C and 410 °C, which can be attributed to the reduction peaks of Fe_2O_3–Fe_3O_4–Fe.[19] After the addition of SO_4^{2-}, the reduction temperatures of the catalysts are higher than that of FeZr. The $FeS_{10}Zr$ catalyst has only one reduction peak at 519 °C, which is close to the reduction peak of the SZr catalyst, and it is also considered to be the overlapping reduction peaks of the iron oxide and sulphates. The H_2-TPR redox curve of the $FeS_{15}Zr$ catalyst has

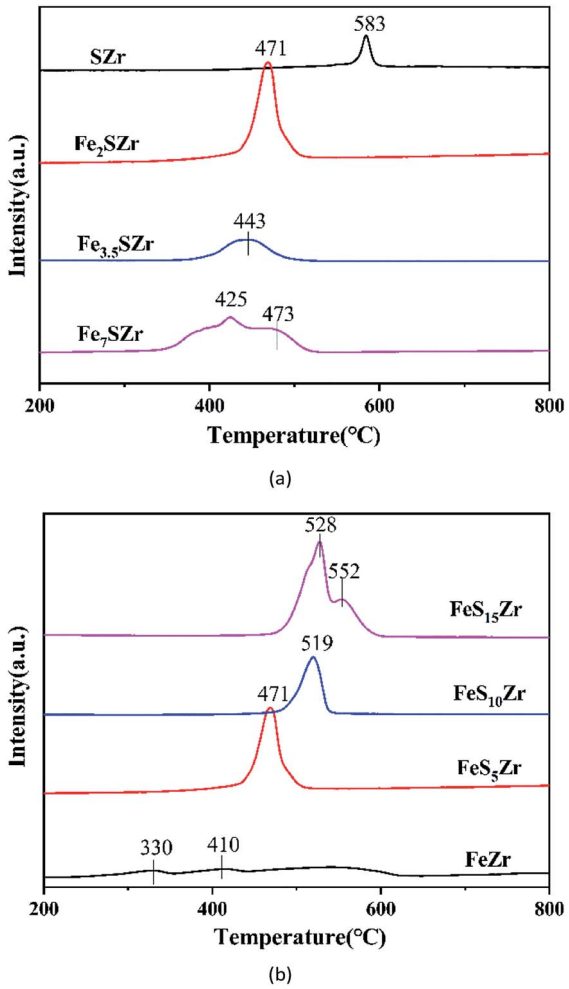

Fig. 3 (a) H_2-TPR of catalysts containing 5% SO_4^{2-} and x% Fe^{3+} ($x = 0$, 2, 3.5, 7). (b) H_2-TPR of catalysts containing 3.5% Fe^{3+} and y% SO_4^{2-} ($y = 0$, 5, 10, 15).

two reduction peaks at 528 °C and 552 °C. The former reduction peak can be attributed to the reduction peak of the iron oxide, while that at 552 °C is considered to be the overlapping reduction peaks of iron oxide and sulphates. According to Fig. 3, it can be concluded that the increase in the Fe^{3+} content in the catalyst caused a shift in the starting reduction temperature of the catalyst to a lower temperature, indicating that an increase in the content of Fe^{3+} increased the redox activity of the catalyst, and the addition of SO_4^{2-} caused the starting reduction temperature of the catalyst to shift to a higher temperature, indicating that the addition of SO_4^{2-} significantly reduced the redox activity of the catalyst.

3.4 XPS

Table 1 shows the atomic concentrations of S, O, Fe and Zr on the surfaces of the different catalysts. Accordingly, when the content of Fe^{3+} was constant, with an increase in SO_4^{2-}, the concentration of Fe atoms on the surface showed a decreasing trend. This is mainly due to the formation of $Fe_2(SO_4)_3$. When the content of SO_4^{2-} was constant, with an increase in Fe_2O_3, the concentration of S atoms on the surface of the catalyst

Table 1 The surface element content in the different catalysts (%)

	FeZr	FeS_5Zr	$FeS_{10}Zr$	$FeS_{15}Zr$	SZr	$Fe_{3.5}SZr$	Fe_7SZr
S 2p	0.000	0.077	0.076	0.091	0.062	0.080	0.066
Zr 3d	0.217	0.161	0.184	0.164	0.212	0.132	0.131
O 1s	0.698	0.719	0.722	0.723	0.726	0.695	0.690
Fe 2p	0.074	0.045	0.018	0.021	0.000	0.093	0.113

increased initially, and then decreased. Similarly, we concluded that more $Fe_2(SO_4)_3$ was produced so that the Fe and S atoms were enriched on the surface. However, when the content of Fe^{3+} increased to a certain level, the SO_4^{2-} on the surface was covered by Fe^{3+}, and thus, the concentration of S atoms on the surface of the catalyst showed the tendency to increase initially, and then decrease with an increase in Fe^{3+}.

The oxidation states of Fe and S on the different catalysts were characterized using XPS, and the results are shown in Fig. 4. The Fe 2p and S bands in Fig. 4 were deconvoluted by searching for the optimal combination with correlation coefficients (R^2) above 0.99 (Origin Pro 8.0). From the curves of Fe 2p, as shown in Fig. 4(a and b), the bonding energies of Fe $2p_{3/2}$ (710–711.5 eV) and Fe $2p_{1/2}$ (724.3–725.5 eV) corresponded well to the references,[29] and the bonding energies of 718.1–719.2 eV corresponded well to the fingerprint peak of Fe^{3+}. Specially, when the content of SO_4^{2-} was 5%, with an increase in Fe^{3+}, the peak with a binding energy at 718.1–719.2 eV became strong, and when the Fe^{3+} content was 3.5%, with an increase in SO_4^{2-}, the peak at 718.1–719.2 eV became weak.

The S 2p XPS spectra for the different catalysts are shown in Fig. 4(c and d). The S 2p XPS spectra of the sulfated catalysts exhibited a main peak at 168.8–170 eV, as shown in Fig. 4. This value is consistent with S^{6+} such as sulfur in SO_4^{2-},[19] indicating that S is in the S^{6+} oxidation state on the catalyst.

3.5 NH_3-temperature programmed desorption (TPD) analysis

The acidity of catalysts plays a very important role in the SCR reaction, and Fe^{3+} and sulphates can provide acidic sites, which can improve the acidity of the catalyst. Therefore, the characteristics of NH_3-TPD were analysed for a series of acidified catalysts, as shown in Fig. 5. Fig. 5(a) shows the NH_3-TPD curves for the catalysts with different Fe^{3+} loadings. The SZr catalyst has two desorption peaks at 410 °C and 120 °C. The desorption amount of ammonia at high temperature was much larger than that at low temperature. It has been reported that the desorption at low temperature is mainly physical adsorption or weak chemical adsorption, while the desorption at high temperature is mainly the strong chemical adsorption of NH_3.[30–32] On the Fe_2SZr catalyst, there was a wide NH_3 desorption peak in the range of 80 °C to 500 °C. With the addition of Fe^{3+}, the desorption capacity of $Fe_{3.5}SZr$ at low temperature (90–180 °C) was slightly higher than the desorption at high temperature (>180 °C). Compared to SZr, the desorption peak of the Fe_7SZr catalyst at high temperature (240 °C) shifted to a lower temperature at nearly 170 °C. Thus, it can be concluded that the

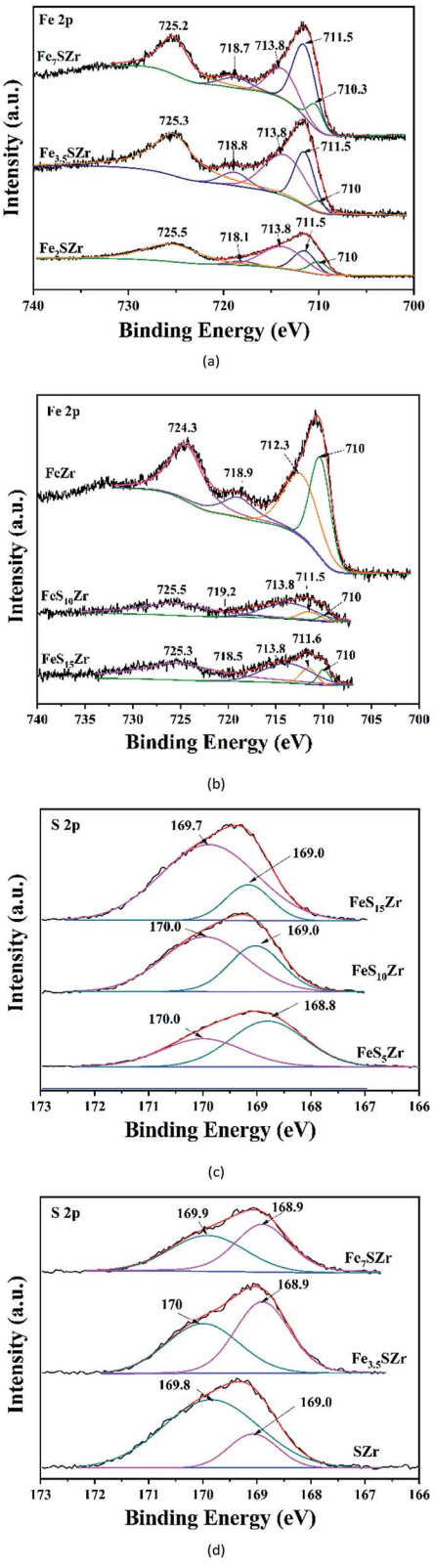

Fig. 4 XPS spectra of different catalysts: (a) XPS-Fe 2p spectra of catalysts containing 5% SO_4^{2-} and x% Fe^{3+} (x = 0, 2, 3.5, 7). (b) XPS-Fe 2p spectra of catalysts containing 3.5% Fe^{3+} and y% SO_4^{2-} (y = 0, 5, 10, 15). (c) XPS-S 2p spectra of catalysts containing 5% SO_4^{2-} and x% Fe^{3+} (x = 0, 2, 3.5, 7). (d) XPS-S 2p spectra of catalysts containing 3.5% Fe^{3+} and y% SO_4^{2-} (y = 0, 5, 10, 15).

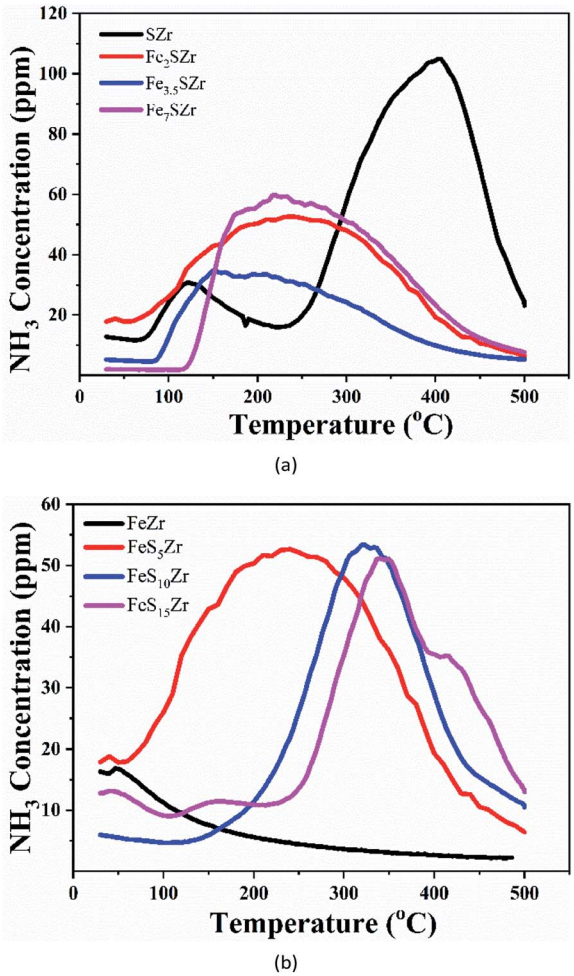

Fig. 5 (a) NH_3-TPD of catalysts containing 5% SO_4^{2-} and x% Fe^{3+} (x = 0, 2, 3.5, 7). (b) NH_3-TPD of catalysts containing 3.5% Fe^{3+} and y% SO_4^{2-} (y = 0, 5, 10, 15).

addition of Fe_2O_3 reduced the ability of the catalyst to adsorb ammonia at high temperatures and improved the ability of the catalyst to adsorb ammonia at moderate and low temperatures. Fig. 5(b) shows the NH_3-TPD curves for the catalysts with different amounts of sulphates. As shown, only a small amount of physically adsorbed ammonia was released on the FeZr catalyst. The addition of 5% sulphate greatly increased the adsorption amount of NH_3. With an increase in the amount of sulphate, the desorption peak of ammonia obviously shifted towards a higher temperature, and the $FeS_{15}Zr$ catalyst showed a desorption peak at 410 °C, which is consistent with the desorption peak of the SZr catalyst, but the desorption amount of ammonia was much less than that of the SZr catalyst. Thus, the addition of SO_4^{2-} increased the adsorption of ammonia on the catalyst at high temperatures and reduced the amount of ammonia adsorbed by the catalyst at moderate or low temperatures.

3.6 NO + O_2-TPD

Fig. 6 shows the NO_x-TPD curve for a series of acidified catalysts. As shown in Fig. 6(a), the SZr catalyst mainly has a nitrogen

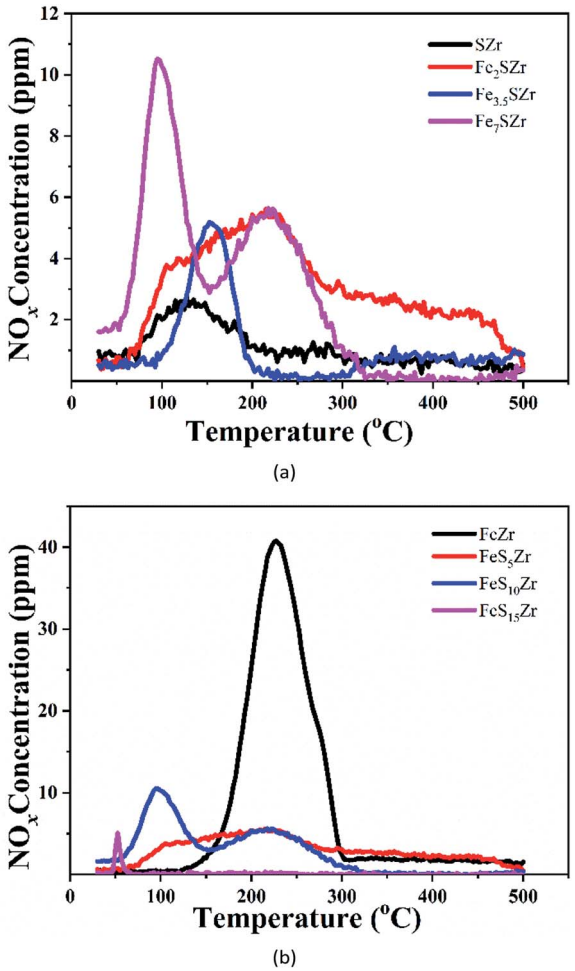

Fig. 6 (a) NO + O_2-TPD of catalysts containing 5% SO_4^{2-} and x% Fe^{3+} ($x = 0$, 2, 3.5, 7). (b) The NO + O_2-TPD of catalysts containing 3.5% Fe^{3+} and y% SO_4^{2-} ($y = 0$, 5, 10, 15).

oxide desorption peak at 120 °C with a low desorption amount. After the addition of 2% Fe^{3+}, nitrogen oxides were desorbed from 100 °C to 500 °C, and the amount of nitrogen oxides desorbed was greatly enhanced. When the addition of Fe^{3+} reached 3.5%, the desorption peak shifted to a higher temperature by approximately 40 °C, but the desorption amount was significantly reduced. When the addition of Fe^{3+} reached 7%, two desorption peaks at 90 °C and 230 °C existed, and the desorption amount was greater than that of the Fe_2SZr catalyst. As shown in Fig. 6(b), the FeZr catalyst has a nitrogen oxide desorption peak at 240 °C with the highest amount of desorption. The addition of 5% SO_4^{2-} to the catalyst significantly decreased the desorption of nitrogen oxides, indicating that SO_4^{2-} had an inhibitory effect on the adsorption of nitrogen oxides. The further addition of SO_4^{2-} to the $FeS_{10}Zr$ catalyst significantly increased the adsorption of nitrogen oxides at low temperature, but decreased the adsorption of nitrogen oxides at high temperature. When the addition of SO_4^{2-} reached 15%, the adsorption of nitrogen oxides was basically completely suppressed. Because NO can be easily oxidized into NO_2 in the presence of O_2, and NO together with NO_2 are both acidic gases, the addition of Fe^{3+} to the catalyst enhanced its adsorption capacity of nitrogen oxides, while the addition of SO_4^{2-} to the catalyst will inhibited the adsorption capacity of nitrogen oxides. However, due to the synergistic effect between Fe^{3+} and SO_4^{2-}, the desorption amount of nitrogen oxides of the $Fe_{3.5}SZr$ catalyst was much less than that of the Fe_2SZr catalyst.

3.7 *In situ* diffuse reflectance infrared Fourier transform spectroscopy (DRIFTS)

3.7.1 NH_3 species adsorbed on the different catalysts. Fig. 7(a) shows the infrared spectra of a series of catalysts containing 5% SO_4^{2-} and different amounts of Fe^{3+} with the saturated adsorption of NH_3 at 30 °C and after purging with N_2. According to the different reports in the literature and the comparative analysis,[26] the region of 3400–2800 cm^{-1} should be

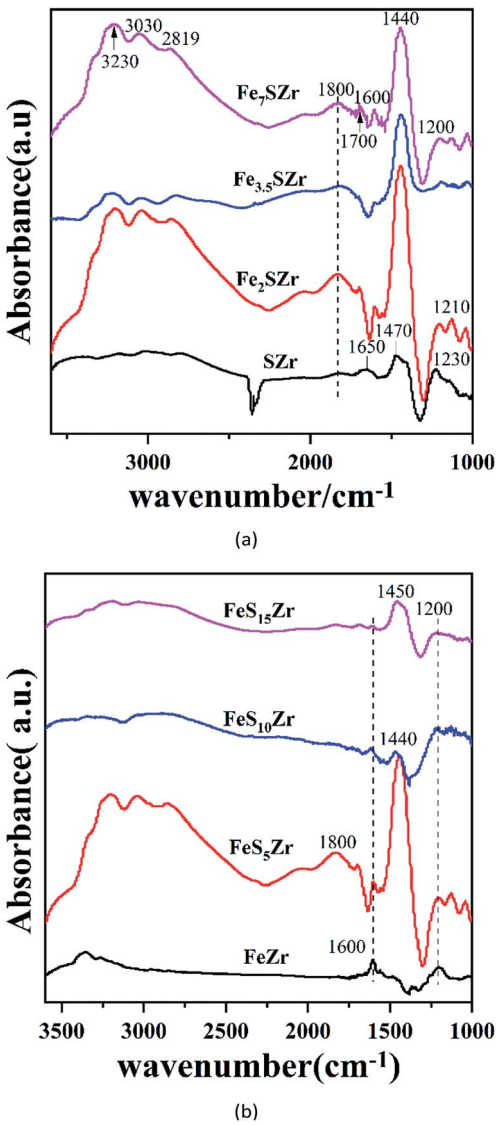

Fig. 7 Infrared spectra of a series of catalysts with the saturated adsorption of NH_3 at 30 °C and after purging with N_2: (a) catalysts containing 5% SO_4^{2-} and x% Fe^{3+} ($x = 0$, 2, 3.5, 7) and (b) catalysts containing 3.5% Fe^{3+} and y% SO_4^{2-} ($y = 0$, 5, 10, 15).

responsible for the NH stretching vibration, which can be considered as the coordination adsorption formed between NH_3 and the oxygen atoms of the metal oxide on the catalyst surface by hydrogen bonding. The absorption at 1600 cm^{-1} is the antisymmetric stretching vibration absorption peak of the NH_3 species adsorbed at the Lewis acid sites, while the peaks at 1230, 1210 and 1200 cm^{-1} are attributed to the symmetric stretching vibration absorption peaks of the NH_3 species adsorbed at the Lewis acid sites. The peaks at 1440, 1470, 1650, and 1700 cm^{-1} are attributed to the anti-symmetric and symmetric stretching vibration absorption peaks of the NH_4^+ species adsorbed at the Brönsted acid sites.[33] It is worth noting that the absorption peak at 1800 cm^{-1} is not attributed to the absorption of NH_3 or NH_4^+ with an increase in the amount of Fe^{3+}. The increase in the amount of Fe^{3+} led to the anti-symmetric stretching vibration absorption peak of the NH_3 species adsorbed at the Lewis acid sites. Simultaneously, we found that with a further increase in the amount of Fe^{3+}, the amount of NH_4^+ species adsorbed at the Brönsted acid sites first increased and then decreased. As shown in Fig. 7(b), the increase in the amount of SO_4^{2-} significantly increased the anti-symmetric and symmetric stretching vibration absorption peaks of the NH_4^+ species adsorbed at the Brönsted acid sites, but a further increase in the amount of SO_4^{2-} did not continue to increase the NH_4^+ species adsorbed at the Brönsted acid sites, which decreased instead, and this may be due to the synergistic effect of iron and SO_4^{2-}.

3.7.2 The NO_x species adsorbed on the surfaces of the different catalysts. Fig. 8(a) shows the infrared spectra of a series of catalysts containing 5% SO_4^{2-} and different amounts of Fe^{3+} with the saturated adsorption of NO + O_2 at 30 °C and after purging with N_2. At 30 °C, the nitrogen oxide vibration absorption peaks appeared at 1630, 1560, 1440, 1280, 1260 and 1240 cm^{-1}. According to the literature,[34–37] the vibration absorption peaks at 1630 and 1560 cm^{-1} are attributed to the vibration absorption of the bridged and bidentate nitrate species adsorbed on the catalyst, respectively, and the vibration absorption peaks at 1440, 1280, 1260 and 1240 cm^{-1} are attributed to the linear nitrate species adsorbed on the catalyst. With the addition of Fe^{3+}, the vibration absorption peak of the linear nitrate species at 1440 cm^{-1} increased, and the anti-symmetric and symmetric vibration absorption peaks of nitrogen oxides at 1230 cm^{-1} disappeared, showing that the linear nitrate species adsorbed at 1260 cm^{-1}. Combined with the NO-TPD results, with the addition of Fe^{3+}, the catalyst could readily adsorb the unstable nitrate species (*e.g.*, linear nitrates), and the desorption temperatures of all the adsorbed nitrates shifted towards a lower temperature. Fig. 8(b) shows the infrared spectra of a series of catalysts containing 3.5% Fe^{3+} and different amounts of SO_4^{2-} with the saturated adsorption of NO + O_2 at 30 °C and after purging with N_2. With the addition of SO_4^{2-} to the catalyst, the NO_2 species (1620 cm^{-1}) and the linear nitrate species (1280 cm^{-1}) on the catalyst surface were reduced, and the vibration absorption peak of the nitrate species showed a red-shift (from 1520 cm^{-1} to 1580 cm^{-1}), with a stable nitrate species appearing at 1440 cm^{-1}. The addition of SO_4^{2-} inhibited the adsorption of nitrogen oxides on the catalyst, which is consistent with the NO_x-TPD results.

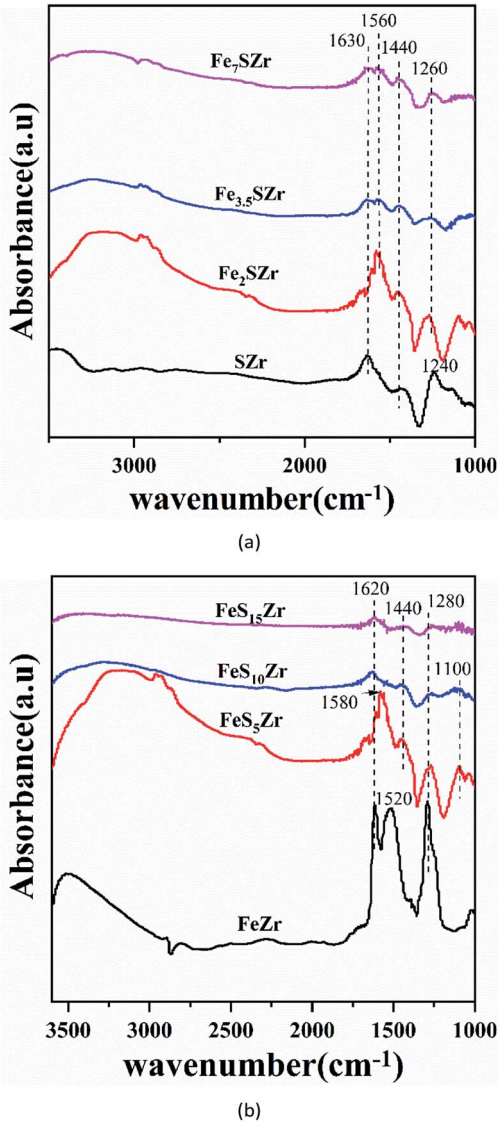

Fig. 8 Infrared spectra of a series of catalysts with the saturated adsorption of NO + O_2 at 30 °C and after purging with N_2: (a) shows catalysts containing 5% SO_4^{2-} and *x*% Fe^{3+} (*x* = 0, 2, 3.5, 7) and (b) catalysts containing 3.5% Fe^{3+} and *y*% SO_4^{2-} (*y* = 0, 5, 10, 15).

3.7.3 Transient DRIFTS for the Fe_7S_5Zr and $Fe_2S_{15}Zr$ catalysts. To better understand the SCR reaction on the sulphated catalysts at high temperature and comparatively analyse the effects of additional Fe^{3+} and SO_4^{2-} on the mechanism of the NH_3-SCR catalytic reaction, we investigated the transient DRIFTS for the Fe_7SZr and $FeS_{15}Zr$ catalysts.

3.7.3.1 Transient DRIFTS of the surface of the Fe_7SZr catalyst at 300 °C. Fig. 9(a) shows the profile of the time-dependent changes of the adsorbed species on the surface of the Fe_7SZr catalyst at 300 °C after introducing NH_3 with the saturated adsorption of NO + O_2. Accordingly, after the adsorption of NO + O_2 on the catalyst surface was saturated, the adsorption peaks appeared at 1620, 1370 and 1140 cm^{-1}. The surface of the catalyst was mainly covered by NO_2 species (1620 cm^{-1}) and nitrate species (1370 and 1140 cm^{-1}).[38] After NH_3 was

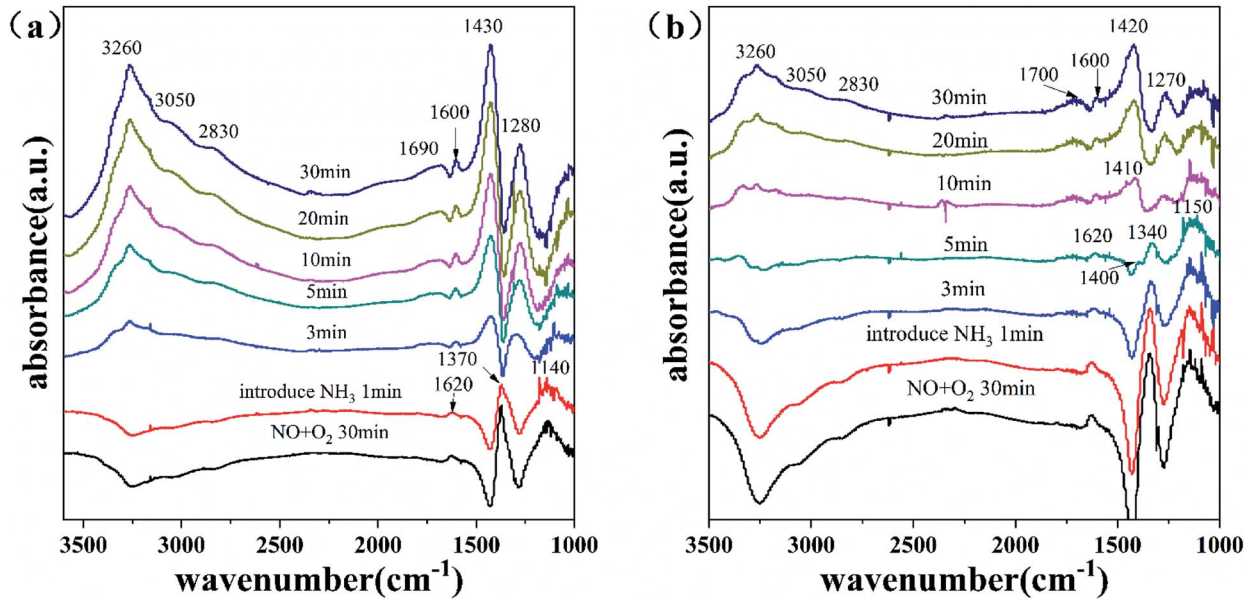

Fig. 9 Profile of the time-dependent changes of the adsorbed species on the surface of different catalysts at 300 °C after introducing NH_3 with the saturated adsorption of NO + O_2 on the (a) Fe_7SZr catalyst and (b) $FeS_{15}Zr$ catalyst.

introduced for 1 min, the adsorbed nitrogen oxide species began to decrease. After 3 min, the absorption peaks of the adsorbed nitrogen oxide species disappeared, and the adsorption peak attributed to the NH_4^+ species at 1430 cm^{-1} appeared, together with the absorption peaks for NH_3 (1280 and 1600 cm^{-1}) and NH_4^+ (1410 and 1690 cm^{-1}) species. After 10 min, the absorption peak of NH_4^+ on the surface of the catalyst gradually increased. These results indicate that the nitrogen oxide species adsorbed on the Fe_7SZr catalyst surface can react rapidly with NH_3 in the gas phase.

Fig. 10(a) shows the profile of the time-dependent changes of the adsorbed species on the surface of the Fe_7SZr catalyst at 300 °C after introducing NO + O_2 with the saturated adsorption of NH_3. When the NH_3 adsorption was saturated, the vibration absorption peaks of NH_3 (1280 cm^{-1}) and NH_4^+ (1680 and 1430 cm^{-1}) on the surface of the catalyst appeared. When NO + O_2 was introduced onto the catalyst surface, the absorption peak of the ammonia species on the surface of the catalyst did not change significantly. After 5 min, the intensities of all the absorption peaks of the adsorbed NH_3 species began to weaken, and even after 30 min, the adsorbed NH_3 species had not reacted completely, and the absorption peak of nitrogen oxide did not appear. This demonstrated that the introduction of NO + O_2 caused a weak reaction with various types of adsorbed NH_3 species on the surface of the catalyst. Thus, combined with Fig. 10(a) and 9(a), at 300 °C the nitrogen oxides adsorbed on the surface of the Fe_7SZr catalyst were the main components that reacted very rapidly with NH_3 in the gaseous state, and the various NH_3 species adsorbed on the surface could also slowly participate in the reaction.

3.7.3.2 Transient DRIFTS of the surface of the $FeS_{15}Zr$ catalyst at 300 °C. Fig. 9(b) shows the profile of the time-dependent changes of the adsorbed species on the surface of the $FeS_{15}Zr$ catalyst at 300 °C after introducing NH_3 with the saturated adsorption of NO + O_2. Accordingly, after the adsorption of NO + O_2 on the catalyst surface was saturated, the adsorption peaks appeared at 1620, 1340 and 1150 cm^{-1}. The surface of the catalyst was mainly covered by NO_2 species (1620 cm^{-1}) and nitrate species (1340 and 1150 cm^{-1}).[39] After NH_3 was introduced, the adsorbed nitrogen oxides species were gradually weakened in 5 min. At the beginning of the 5th minute, the adsorption peak attributed to the NH_4^+ species appeared at 1400 cm^{-1}. At the 10th minute, the absorption peaks of the nitrogen oxide species basically disappeared, and the absorption peaks of NH_3 (1270 and 1600 cm^{-1}) and NH_4^+ (1410 and 1700 cm^{-1}) species appeared. After 10 min, the catalyst surface was covered by various ammonia species, and they gradually increased. These results indicate that the nitrogen oxide species adsorbed on the surface of the $FeS_{15}Zr$ catalyst can react with NH_3 in the gas phase.

Fig. 10(b) shows the profile of the time-dependent changes of the adsorbed species on the surface of the $FeS_{15}Zr$ catalyst at 300 °C after introducing NO + O_2 with the saturated adsorption of NH_3. After NO + O_2 was introduced on the catalyst surface for 5 min, all the adsorbed NH_3 species disappeared. Starting from the 10th minute, the surface was gradually occupied by nitrate. This indicates that NO + O_2 can react with the various NH_3 species adsorbed on the surface. Thus, combined with Fig. 10(b) and 9(b), at 300 °C the NH_3 species adsorbed on the surface of the $FeS_{15}Zr$ catalyst can rapidly react with NO_x in the gas phase, while the nitrogen oxide species adsorbed on the surface can also rapidly react with NH_3 in the gas phase.

Combined with the results of the DRIFTs study of the transient reactions of the Fe_7SZr and $FeS_{15}Zr$ catalysts at 300 °C, it can be concluded that there are two NH_3-SCR reaction paths on the surface of the sulphated iron-based catalyst at 300 °C, namely a Langmuir–Hinshelwood[15] reaction mechanism and an Eley–Rideal[27,33] reaction mechanism, that is,

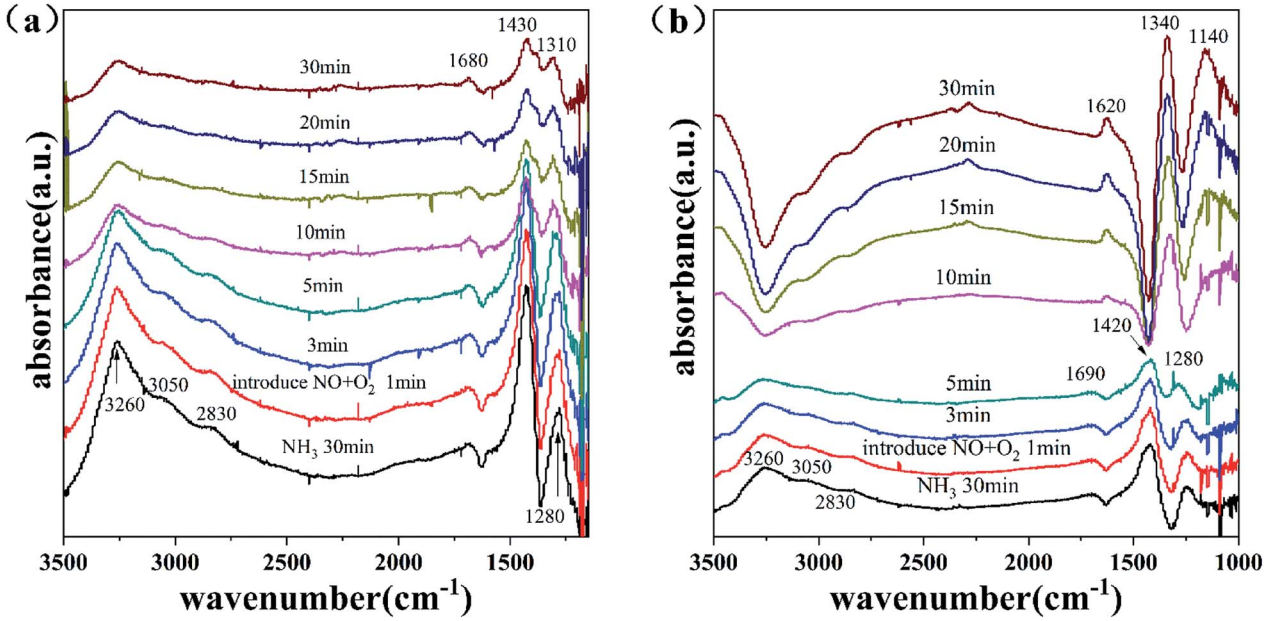

Fig. 10 Profile of the time-dependent changes of the adsorbed species on the surface of different catalysts at 300 °C after introducing NO + O_2 with the saturated adsorption of NH_3 on the (a) Fe_7SZr catalyst and (b) $FeS_{15}Zr$ catalyst.

NH_3 adsorption on the catalyst surface. NO is first oxidized into NO_2 to be adsorbed on the surface of the catalyst to produce nitrates or nitrite species, and the NH_3 species adsorbed on the surface can react with both gaseous NO_x and the adsorbed NO_x species to produce N_2 and H_2O. The nitrogen oxide species adsorbed on the surface of the Fe_7SZr catalyst can react very rapidly with the gaseous NH_3, while various NH_3 species adsorbed on the surface can also slowly participate in the reaction, indicating that when the amount of Fe_2O_3 in the catalyst increases, the SCR reaction occurring on the catalyst obviously follows the Langmuir–Hinshelwood reaction path, with a small portion of the reaction following the Eley–Rideal reaction mechanism simultaneously. The NH_3 species adsorbed on the surface of the $FeS_{15}Zr$ catalyst at 300 °C can rapidly react with the NO_x in the gas phase, and the nitrogen oxides species adsorbed on the surface can also rapidly react with the NH_3 in the gas phase. This indicates that when the amount of SO_4^{2-} in the catalyst increases, the SCR reaction on the surface of the catalyst obviously follows the Eley–Rideal reaction mechanism, mainly because the increase in the amount of SO_4^{2-} significantly enhances the ammonia adsorption capacity of the catalyst at a high temperature, while reducing the adsorption of nitrogen oxides, which is conducive to enhancing the NH_3 adsorption by the catalyst, thereby promoting the SCR reaction at high temperature. This is consistent with the results of the activity test for the catalyst with varying amounts of SO_4^{2-}.

4. The synergistic mechanism of Fe^{3+} and sulphates for NH_3-SCR

The roles of Fe^{3+} and sulphates were very different at low temperature and high temperature. When the SO_4^{2-} content is constant, the addition of Fe^{3+} to the catalyst will enhance its adsorption capacity of nitrogen oxides and NH_3 species at moderate and low temperatures. According to the references,[27,33,40,41] the mechanism of the SCR generally follows the Langmuir–Hinshelwood reaction path at moderate and low temperatures, and thus the Fe^{3+} obviously adsorbed NH_3 and oxidized it to $-NH_2$, which is the important intermediate species for the SCR reaction[42–46] and can react with the NO oxidation species (NO_2^- and NO_3^-) to form the intermediate species, and then decompose to N_2 and H_2O. Thus, the addition of Fe^{3+} improved the redox ability, which affected the activity for the SCR at moderate and low temperatures. However, at high temperature, an increase in the amount of Fe^{3+} will promote the oxidation of NH_3 because it can increase the redox activity of the catalyst, which results in a decrease in the efficiency of the catalytic reduction of nitrogen oxides. When the content of Fe^{3+} is constant, with an increase in the content of SO_4^{2-}, the concentration of Fe^{3+} on the surface showed a decreasing trend because of the formation of $Fe_2(SO_4)_3$, which leads to the complete inhibition of the adsorption of NO_x and NH_3 to reduce the conversion of NO_x in NH_3-SCR at moderate and low temperature. At high temperature, the redox activity of the catalyst is reduced with the addition of SO_4^{2-}, which restrains the oxidation reaction of NH_3 on the catalyst. Meanwhile, the significant increase in NH_4^+ species adsorbed at the Brönsted acid sites improves the activity for the SCR, which follows the Eley–Rideal reaction path. Overall, the effect on the SCR for Fe^{3+} and SO_4^{2-} was restrained by each of them, and thus only the appropriate contents of Fe^{3+} and SO_4^{2-} could result in high activity in the temperature range of 300–450 °C. Similar to oxide catalysts such as Mo–Fe,[47] W–Fe,[48] W–Ce,[49] and Mo–Fe[50] oxides, the sulphated iron-based catalysts possess acid-redox dinuclear sites, where Fe^{3+} is the redox site and SO_4^{2-} is the acid site. The

interfaces of the acid-redox sites are key to the SCR reaction activities. Thus, designing catalysts to optimize the interaction between the acid-redox sites is an effective measure to control NO emissions.

5. Conclusions

Different sulphated iron-based catalysts with various loadings of Fe^{3+} and SO_4^{2-} on ZrO_2 were prepared *via* the incipient wetness method, and investigated for the selective catalytic reduction (SCR) of NO_x by ammonia. Compared to all the catalysts, the Fe_2SZr catalyst could achieve above 90% NO_x removal efficiency at 350–450 °C, and the main reactions on its surface were the NH_3-SCR reaction and the oxidation of NH_3. Meanwhile, the interaction between Fe^{3+} and SO_4^{2-} was found to affect the redox ability, acid sites, adsorption of NO_x and NH_3, and play a role in the SCR activity. Specifically, increasing the content of Fe^{3+} improved the redox activity of the catalyst and enhanced the adsorption of ammonia at medium and low temperatures. In addition, increasing the amount of Fe^{3+} promoted the oxidation of NH_3 at high temperatures, which led to a reduction in the efficiency of NO_x conversion. With an increase in SO_4^{2-}, the concentration of Fe^{3+} on the surface of the catalyst showed a decreasing trend because of the formation of $Fe_2(SO_4)_3$, which inhibited the adsorption of NO_x and NH_3 and reduced the NO_x conversion of the NH_3-SCR at medium and low temperatures. At high temperatures, the addition of SO_4^{2-} reduced the redox activity of the catalyst and inhibited the oxidation reaction of NH_3. Meanwhile, the significant increase in NH_4^+ species adsorbed on the Brönsted acid sites improved the SCR activity because the main reaction pathway over the Fe_xS_yZr catalyst follows the Eley–Rideal mechanism at high temperatures.

Conflicts of interest

There are no conflicts to declare.

Acknowledgements

This work was financially supported by the National High-Tech Research and Science and Technology Plan Program of Hebei Province (Grant No. 206Z3702G) and Development (Air Pollution Control Technology Research) Program of China (Grant No. 2016YFC0205302 and No. 2016YFC0205300) and National Natural Science Fund of China (Grant No. 21507100).

References

1 Z. Fu, M. Guo, C. Liu, N. Ji, C. Song and Q. Liu, Design and Synthesis Functional Selective Catalytic Reduction Catalyst for NOx Removal, *Procedia Eng.*, 2015, **121**, 952–956.
2 M. Jabłońska and R. Palkovits, Copper based catalysts for the selective ammonia oxidation into nitrogen and water vapour—Recent trends and open challenges, *Appl. Catal., B*, 2016, **181**, 332–351.
3 G. Busca, L. Lietti, G. Ramis and F. Berti, Chemical and mechanistic aspects of the selective catalytic reduction of NOx by ammonia over oxide catalysts: a review, *Appl. Catal., B*, 1998, **18**, 1–36.
4 A. Boubnov, H. W. P. Carvalho, D. E. Doronkin, T. Guenter, E. Gallo, A. J. Atkins, C. R. Jacob and J. D. Grunwaldt, Selective Catalytic Reduction of NO Over Fe-ZSM-5: Mechanistic Insights by Operando HERFD-XANES and Valence-to-Core X-ray Emission Spectroscopy, *J. Am. Chem. Soc.*, 2014, **136**, 13006–13015.
5 D. Jo, G. T. Park, T. Ryu and S. B. Hong, Economical synthesis of high-silica LTA zeolites: a step forward in developing a new commercial NH3-SCR catalyst, *Appl. Catal., B*, 2019, **243**, 212–219.
6 J. Mu, X. Li, W. Sun, S. Fan, X. Wang, L. Wang, M. Qin, G. Gan, Z. Yin and D. Zhang, Inductive Effect Boosting Catalytic Performance of Advanced Fe1–xVxOδ Catalysts in Low-Temperature NH3 Selective Catalytic Reduction: Insight into the Structure, Interaction, and Mechanisms, *ACS Catal.*, 2018, **8**, 6760–6774.
7 P. Fabrizioli, T. Bürgi and A. Baiker, Environmental Catalysis on Iron Oxide–Silica Aerogels: Selective Oxidation of NH3 and Reduction of NO by NH3, *J. Catal.*, 2002, **206**, 143–154.
8 S. Ding, F. Liu, X. Shi and H. Hong, Promotional effect of Nb additive on the activity and hydrothermal stability for the selective catalytic reduction of NOx with NH3 over CeZrOx catalyst, *Appl. Catal., B*, 2016, **180**, 766–774.
9 C. Sun, H. Liu, W. Chen, D. Chen, S. Yu, A. Liu, L. Dong and S. Feng, Insights into the Sm/Zr co-doping effects on N2 selectivity and SO2 resistance of a MnOx-TiO2 catalyst for the NH3-SCR reaction, *Chem. Eng. J.*, 2018, **347**, 27–40.
10 S. Yang, F. Qi, S. Xiong, D. Hao and J. Li, MnOx supported on Fe-Ti spinel: a novel Mn based low temperature SCR catalyst with a high N2 selectivity, *Appl. Catal., B*, 2016, **181**, 570–580.
11 R. Zhang, Y. Li and T. Zhen, Ammonia selective catalytic reduction of NO over Fe/Cu-SSZ-13, *RSC Adv.*, 2014, **4**, 52130–52139.
12 F. Cao, S. Su, J. Xiang, P. Wang, S. Hu, L. Sun and A. Zhang, The activity and mechanism study of Fe-Mn-Ce/γ-Al_2O_3 catalyst for low temperature selective catalytic reduction of NO with NH_3, *Fuel*, 2015, **139**, 232–239.
13 B. Shen, T. Liu, N. Zhao and X. Yang, Iron-doped Mn-Ce/TiO2 catalyst for low temperature selective catalytic reduction of NO with NH3, *J. Environ. Sci.*, 2010, **22**, 1447–1454.
14 W. Zhao, C. Li, P. Lu, Q. Wen, Y. Zhao, X. Zhang, C. Fan and S. Tao, Iron, lanthanum and manganese oxides loaded on γ-Al2O3 for selective catalytic reduction of NO with NH3 at low temperature, *Environ. Technol.*, 2013, **34**, 81–90.
15 G. Zhou, B. Zhong, W. Wang, X. Guan, B. Huang, D. Ye and H. Wu, In situ DRIFTS study of NO reduction by NH3 over Fe–Ce–Mn/ZSM-5 catalysts, *Catal. Today*, 2011, **175**, 157–163.
16 Y. Xia, W. Zhan, Y. Guo, Y. Guo and G. Lu, Fe-Beta zeolite for selective catalytic reduction of NOx with NH3: influence of Fe content, *Chin. J. Catal.*, 2016, **37**, 2069–2078.
17 Z. Ma, H. Yang, L. Qian, J. Zheng and X. Zhang, Catalytic reduction of NO by NH3 over Fe–Cu–OX/CNTs-TiO2

composites at low temperature, *Appl. Catal., A*, 2012, **427–428**, 43–48.

18 T. Gu, L. Yue, X. Weng, H. Wang and Z. Wu, The enhanced performance of ceria with surface sulfation for selective catalytic reduction of NO by NH3, *Catal. Commun.*, 2010, **12**, 310–313.

19 M. Lei, J. Li, K. Rui and L. Fu, Catalytic Performance, Characterization, and Mechanism Study of Fe2(SO4)3/TiO2 Catalyst for Selective Catalytic Reduction of NOx by Ammonia, *J. Phys. Chem. C*, 2011, **115**, 7603–7612.

20 H. Zhang, Y. Zou and Y. Peng, Influence of sulfation on CeO2-ZrO2 catalysts for NO reduction with NH3, *Chin. J. Catal.*, 2017, **38**, 160–167.

21 Q. Lu, W. Yun, D. Pang, O. Feng and C. Zhang, SO42–Mn-Co-Ce supported on TiO2/SiO2 with high sulfur durability for low-temperature SCR of NO with NH3, *Catal. Commun.*, 2016, **78**, 22–25.

22 Q. Zhang, J. Zhang, Z. Song, N. Ping and L. Xin, A novel and environmentally friendly SO42–/CeO2 catalyst for the selective catalytic reduction of NO with NH3, *J. Ind. Eng. Chem.*, 2016, **34**, 165–171.

23 Y. Yu, J. Chen, J. Wang and Y. Chen, Performances of CuSO4/TiO2 catalysts in selective catalytic reduction of NOx by NH3, *Chin. J. Catal.*, 2016, **37**, 281–287.

24 T. Xu, X. Wu, X. Liu, L. Cao, Q. Lin and D. Weng, Effect of barium sulfate modification on the SO2 tolerance of V2O5/TiO2 catalyst for NH3-SCR reaction, *J. Environ. Sci.*, 2017, **57**, 110–117.

25 X. Du, X. Wang, Y. Chen, X. Gao and L. Zhang, Supported metal sulfates on Ce–TiOx as catalysts for NH3–SCR of NO: high resistances to SO2 and potassium, *J. Ind. Eng. Chem.*, 2016, **36**, 271–278.

26 L. Jian, Z. Zhen, J. Wang, C. Xu, A. Duan, G. Jiang and Q. Yang, The highly active catalysts of nanometric CeO2-supported cobalt oxides for soot combustion, *Appl. Catal., B*, 2008, **84**, 185–195.

27 N. Apostolescu, B. Geiger, K. Hizbullah, M. T. Jan, S. Kureti, D. Reichert, F. Schott and W. Weisweiler, Selective catalytic reduction of nitrogen oxides by ammonia on iron oxide catalysts, *Appl. Catal., B*, 2006, **62**, 104–114.

28 X. Wang, S. Wu, W. Zou, S. Yu and L. Dong, Fe-Mn/Al2O3 catalysts for low temperature selective catalytic reduction of NO with NH3, *Chin. J. Catal.*, 2016, **37**, 1314–1323.

29 S. Yang, C. Liu, H. Chang, L. Ma, Z. Qu, N. Yan, C. Wang and J. Li, Improvement of the Activity of γ-Fe2O3 for the Selective Catalytic Reduction of NO with NH3 at High Temperatures: NO Reduction versus NH3 Oxidization, *Ind. Eng. Chem. Res.*, 2013, **52**, 5601–5610.

30 R. Q. Long and R. T. Yang, Selective Catalytic Oxidation of Ammonia to Nitrogen over Fe2O3–TiO2 Prepared with a Sol–Gel Method, *J. Catal.*, 2002, **207**, 158–165.

31 L. S. Cheng, R. T. Yang and C. Ning, Iron Oxide and Chromia Supported on Titania-Pillared Clay for Selective Catalytic Reduction of Nitric Oxide with Ammonia, *J. Catal.*, 1996, **164**, 70–81.

32 R. Q. Long and R. T. Yang, The promoting role of rare earth oxides on Fe-exchanged TiO 2-pillared clay for selective catalytic reduction of nitric oxide by ammonia, *Appl. Catal., B*, 2000, **27**, 87–95.

33 G. Ramis, L. Yi, G. Busca, M. Turco, E. Kotur and R. J. Willey, Adsorption, Activation, and Oxidation of Ammonia over SCR Catalysts, *J. Catal.*, 1995, **157**, 523–535.

34 A. Bourane, O. Dulaurent, S. Salasc, C. Sarda, C. Bouly and D. Bianchi, Heats of Adsorption of Linear NO Species on a Pt/Al2O3 Catalyst Using in Situ Infrared Spectroscopy under Adsorption Equilibrium, *J. Catal.*, 2001, **204**, 77–88.

35 A. Kotsifa, D. I. Kondarides and X. E. Verykios, Comparative study of the chemisorptive and catalytic properties of supported Pt catalysts related to the selective catalytic reduction of NO by propylene, *Appl. Catal., B*, 2007, **72**, 136–148.

36 W. Schieer, H. Vinek and A. Jentys, Surface species during catalytic reduction of NO by propene studied by in situ IR-spectroscopy over PT supported on mesoporous Al2O3 with MCM-41 type structure, *Appl. Catal., B*, 2001, **33**, 263–274.

37 M. A. Larrubia, G. Ramis and G. Busca, An FT-IR study of the adsorption and oxidation of N-containing compounds over Fe 2O3-TiO2 SCR catalysts, *Appl. Catal., B*, 2001, **30**, 101–110.

38 L. J. France, Q. Yang, W. Li, Z. Chen, J. Guang, D. Guo, L. Wang and X. Li, Ceria modified FeMnOx—Enhanced performance and sulphur resistance for low-temperature SCR of NOx, *Appl. Catal., B*, 2017, **206**, 203–215.

39 T. Venkov, K. Hadjiivanov and D. Klissurski, IR spectroscopy study of NO adsorption and NO + O2 co-adsorption on Al2O3, *Phys. Chem. Chem. Phys.*, 2002, **4**, 2443–2448.

40 J. Liu, X. Li, R. Li, Q. Zhao, J. Ke, H. Xiao, L. Wang, S. Liu, M. Tadé and S. Wang, Facile synthesis of tube-shaped Mn-Ni-Ti solid solution and preferable Langmuir-Hinshelwood mechanism for selective catalytic reduction of NO by NH3, *Appl. Catal., A*, 2018, **549**, 289–301.

41 J. Liu, G.-q. Li, Y.-f. Zhang, X.-q. Liu, Y. Wang and Y. Li, Novel Ce-W-Sb mixed oxide catalyst for selective catalytic reduction of NOx with NH3, *Appl. Surf. Sci.*, 2017, **401**, 7–16.

42 J. Fan, P. Ning, Z. Song, X. Liu, L. Wang, J. Wang, H. Wang, K. Long and Q. Zhang, Mechanistic aspects of NH3-SCR reaction over CeO2/TiO2-ZrO2-SO42– catalyst: in situ DRIFTS investigation, *Chem. Eng. J.*, 2018, **334**, 855–863.

43 J. Zhang, X. Li, P. Chen and B. Zhu, Research Status and Prospect on Vanadium-Based Catalysts for NH(3)-SCR Denitration, *Materials*, 2018, **11**, 1632.

44 J. Liu, R.-t. Guo, M.-y. Li, P. Sun, S.-m. Liu, W.-g. Pan, S.-w. Liu and X. Sun, Enhancement of the SO2 resistance of Mn/TiO2 SCR catalyst by Eu modification: a mechanism study, *Fuel*, 2018, **223**, 385–393.

45 J.-W. Shi, Y. Wang, R. Duan, C. Gao, B. Wang, C. He and C. Niu, The synergistic effects between Ce and Cu in CuyCe1–yW5Ox catalysts for enhanced NH3-SCR of NOx and SO2 tolerance, *Catal. Sci. Technol.*, 2019, **9**, 718–730.

46 H. Wang, P. Ning, Y. Zhang, Y. Ma, J. Wang, L. Wang and Q. Zhang, Highly efficient WO3-FeOx catalysts synthesized using a novel solvent-free method for NH3-SCR, *J. Hazard. Mater.*, 2020, **388**, 121812.

47 Y. Xin, N. Zhang, Q. Li, Z. Zhang, X. Cao, L. Zheng, Y. Zeng and J. A. Anderson, Active Site Identification and Modification of Electronic States by Atomic-Scale Doping To Enhance Oxide Catalyst Innovation, *ACS Catal.*, 2018, **8**, 1399–1404.

48 Z. Liu, H. Su, B. Chen, J. Li and S. I. Woo, Activity enhancement of WO3 modified Fe2O3 catalyst for the selective catalytic reduction of NOx by NH3, *Chem. Eng. J.*, 2016, **299**, 255–262.

49 J. Chen, Y. Chen, M. Zhou, Z. Huang, J. Gao, Z. Ma, J. Chen and X. Tang, Enhanced Performance of Ceria-Based NOx Reduction Catalysts by Optimal Support Effect, *Environ. Sci. Technol.*, 2017, **51**, 473–478.

50 W. Qu, X. Liu, J. Chen, Y. Dong, X. Tang and Y. Chen, Single-atom catalysts reveal the dinuclear characteristic of active sites in NO selective reduction with NH3, *Nat. Commun.*, 2020, **11**, 1532.